International Conference on Applied Energy 2020
Dec. 1 - Dec. 10, 2020, Bangkok / Virtual
Paper ID: 0055

Performance estimation of a V-shape perovskite-silicon tandem device composed of a bifacial heterojunction silicon cell

Likai Zheng, Yimin Xuan *

School of Energy and Power Engineering, Nanjing University of Aeronautics and Astronautics, Nanjing 210016, P. R. China.
*Corresponding author: ymxuan@nuaa.edu.cn (Y. Xuan)

ABSTRACT

Coupling perovskite solar cells (PSCs) and silicon solar cells (SSCs) in a V-shape tandem configuration is a promising strategy for efficient solar energy splitting utilization that requires no beam splitter mirror and only half usage amount of SSCs. Here we develop a method for the performance estimation of a V-shape tandem device, which employs a 23%-efficient practical heterojunction SSC as a sub-cell for demonstration. The investigation results of influences of PSCs' bandgap, layer thicknesses and transparent electrode materials on the tandem performance provide a guidance in selecting and optimizing of PSCs for getting most energy output. The tungsten-doped indium oxide is proved to be the suitable material for PSCs in V-shape devices.

Keywords: perovskite/silicon tandem device, solar energy photovoltaic utilization, bifacial HIT solar silicon cell, spectral efficiency.

NONMENCLATURE

Abbreviations	
HIT	Heterojunction with intrinsic thin film
PSC	Perovskite solar cell
SSC	Silicon solar cell
TCO	Transparent conductive oxide
ITO	Tin-doped indium oxide
IWO	Tungsten-doped indium oxide
EQE	External quantum efficiency
FDTD	Finite difference time domain
S-Q limit	Shockley-Quiese limit
4-T	Four-terminal
Symbols	
J_{SC}	Short-circuit current density
V_{OC}	Open-circuit voltage
FF	Fill factor
η	Efficiency
I	AM1.5G spectral irradiation intensity
λ	Wavelength
λ_g	The wavelength corresponding to the bandgap
P	Power density
E_g	Bandgap
q	Elementary charge
h	Planck's constant
c	Speed of light
C	Fraction of S-Q limit efficiency
f	Ratios of the photon-generated current of a filtered Si cell to that of a unfiltered Si cell
φ_{PSC}	Spectral reflectance of PSC
m	Ideality factor of diode
k	Boltzmann's constant
T	Temperature
V_0	Open-circuit voltage of the front side of a standalone HIT silicon solar cell
J_0	Short-circuit current density of the front side of a standalone HIT silicon solar cell
$\vec{H}$	Magnetic field
$\vec{B}$	Magnetic flux density
$\vec{E}$	Electric field
$\vec{D}$	Electric displacement field
ε	Complex permittivity
μ	Complex permeability

1. INTRODUCTION

In the past decade, PSCs have attracted tremendous attention with rapid improvement of efficiency [1-3]. Owing to multitudinous advantages such as tunable bandgap, strong light absorption, sharp absorption edge

Selection and peer-review under responsibility of the scientific committee of the 12th Int. Conf. on Applied Energy (ICAE2020).

and low costs in fabrication, PSCs are regarded as one of the most promising partners of commercial SSCs for high efficiency tandem technology [4-6]. Among the architectures of perovskite-Si tandem devices, 4-T configurations allow for relatively independent fabrication of the PSCs and SSCs and free the tandem devices from current matching constraints, which are beneficial to pursuit higher efficiency as well as to commercialize with minor adjustment of each production line [7-10]. However, conventional stacked architecture suffers from several problems, such as parasitic and reflective optical losses in the PSCs as well as reduced V_{OC} of Si sub-cells under filtered illumination, which still hinder further promotion of tandem devices efficiency [11, 12]. Coupling bifacial HIT SSCs and low-parasitic-absorption PSCs in a V-shape tandem configuration has been proved as a promising strategy to tackle these problems simultaneously, which needs only half amount of SSCs compared to the conventional configurations [13].

For a tandem device, specific performances of a silicon sub-cell bring specific requirements of a perovskite sub-cell. Numerical model have been reported for detailed performance analysis of the perovskite-silicon tandem devices [14], which requires specific optical and electrical parameters of solar cells. A spectral efficiency concept has been proposed for fast energy performances assessment of general tandem devices without regard to specific structure of solar cells [15, 16]. Nevertheless, a universal method that can provide guidance in selecting and optimizing of specific PSCs needs further development.

In this work, we established a comprehensive approach by coupling spectral efficiency concept and optical simulations for performance estimation of a V-shape tandem device, and a 23%-efficient bifacial HIT SSC was fabricated for demonstration of this method. The maximum possible efficiency of the tandem devices as well as the optimal bandgap of ideal PSCs was calculated. Notably, a factor *f* is introduced to uniformly evaluate the effects of bandgap, layer thicknesses and TCO type (IWO or ITO) of a typical PSC on the tandem performance, pointing out an optimization path of this type of PSCs in a silicon-based V-shape tandem device.

2. EXPERIMENT AND CALCULATION METHODS

2.1 Experiment methods

The bifacial HIT SSC used in this work was fabricated through a production line manufacturing process with the same silver grid pattern on both side. The *J-V* curves were measured using a Keithley 2400 source meter under AM1.5 G illumination with a solar simulator (CrownTech, EASISOLAR-50-3A). The light intensity was calibrated using a standard silicon reference solar cell (CrownTech). The EQE curves were measured using a CrownTech system (QTEST HIFINITY 5) that was calibrated by a certified solar cell (CrownTech) each time before the measurement.

2.2 Calculation methods

2.2.1 Calculation of tandem efficiencies

Figure 1(a) shows the diagram of a V-shape tandem device, consisting of one bifacial HIT SSC and two PSCs with an angle of 45° to both sides of the HIT SSC. Incident light can be reflected by the PSC_1 and PSC_2 onto the front side (n-type) and the rear side (p-type) of the HIT cell, respectively. The efficiencies of V-shape tandem devices can be calculated on the basis of the spectral efficiency concept [16]. The equations were established based on the previous work [13] with minor extensions:

$$\eta_{\text{tandem}} = \eta_{PSC} + \eta_{Si} \quad (1)$$

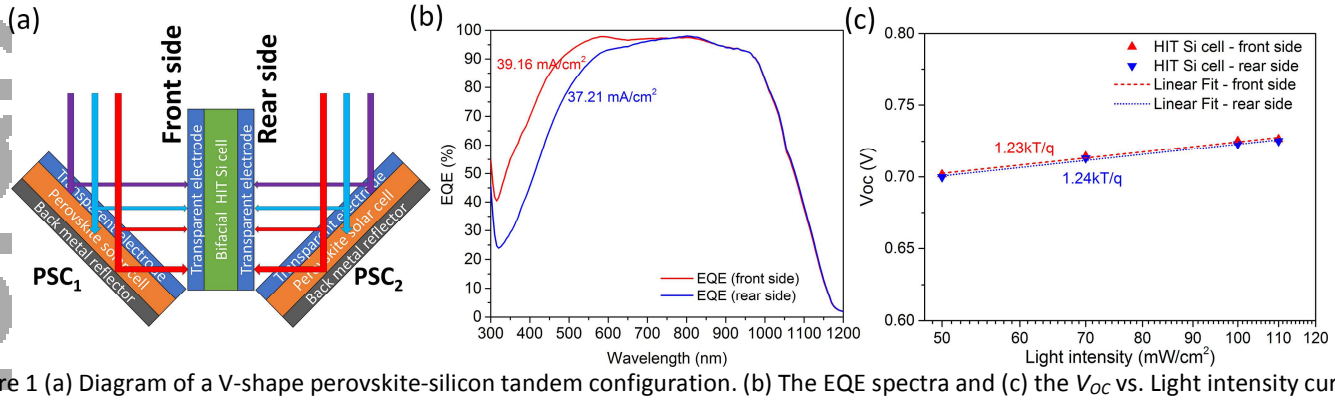

Figure 1 (a) Diagram of a V-shape perovskite-silicon tandem configuration. (b) The EQE spectra and (c) the V_{OC} vs. Light intensity curves of the front and rear sides of a bifacial HIT SSC.

$$\eta_{PSC}=\frac{1}{2}\left[C_1\eta_{S-Q}\left(\lambda_{g1}\right)+C_2\eta_{S-Q}\left(\lambda_{g2}\right)\right] \quad (2)$$

$$\eta_{Si}=\frac{1}{2}\left(P_{nb}+P_{nr}+P_{pb}+P_{pr}\right)\Big/P_{sun} \quad (3)$$

$$P_{sun}=\int_{300\,nm}^{2500\,nm} I(\lambda)\,d\lambda \quad (4)$$

$$\begin{cases} P_{nb}=f_{nb}\int_{300nm}^{\lambda_{g1}}\eta_{Si}^{n}(\lambda)I(\lambda)d\lambda \\ P_{nr}=f_{nr}\int_{\lambda_{g1}}^{1200nm}\eta_{Si}^{n}(\lambda)I(\lambda)d\lambda \\ P_{pb}=f_{pb}\int_{300nm}^{\lambda_{g2}}\eta_{Si}^{p}(\lambda)I(\lambda)d\lambda \\ P_{pr}=f_{pr}\int_{\lambda_{g2}}^{1200nm}\eta_{Si}^{p}(\lambda)I(\lambda)d\lambda \end{cases} \quad (5)$$

The f factor represents the ratio of photon-generated current of filtered Si cell to that of unfiltered Si cell for different sides and different wavebands:

$$f=\int_{\lambda}\varphi_{PSC}(\lambda)J_{SC}(\lambda)d\lambda\Big/\int_{\lambda}J_{SC}(\lambda)d\lambda \quad (6)$$

The subscript characters *n* and *p* correspond to the front and rear side of the HIT solar cell, respectively. The subscript characters *b* and *r* correspond to the integral waveband of 300nm-λ_g and λ_g-1200nm, respectively. The efficiency of HIT SSC can be given as:

$$\eta_{Si}^{n(p)}(\lambda)=V_{OC}\cdot FF\cdot J_{SC}^{n(p)}(\lambda)\Big/I(\lambda) \quad (7)$$

$$J_{SC}^{n(p)}(\lambda)=q\lambda EQE_{Si}^{n(p)}(\lambda)I(\lambda)\Big/hc \quad (8)$$

$$V_{OC}=V_0+\left(mkT/q\right)\ln\left(J_{SC}^{n}+J_{SC}^{p}\Big/J_0\right) \quad (9)$$

2.2.2 Optical simulation of PSCs

The optical performance of the PSCs with specific structures and materials can be obtained by solving the Maxwell's equations below through the FDTD method. More details about the FDTD method can be found in our previous work [17, 18].

$$\begin{cases} \nabla\times\vec{H}=\partial\vec{D}/\partial t \\ \nabla\times\vec{E}=-\partial\vec{B}/\partial t \\ \vec{D}=\varepsilon\vec{E} \\ \vec{B}=\mu\vec{H} \end{cases} \quad (10)$$

3. RESULTS AND DISCUSSION

3.1 *Performances of the bifacial HIT solar cell*

The measured results obtained from the *J-V* curves are summarized in Table 1. The efficiency difference between the rear and front sides is mainly due to the J_{SC} difference. This can be directly observed from the EQE measure results plotted in Figure 1(b). The parasitic absorption of the p-type α-Si:H layer on the rear side is higher than the n-type α-Si:H layer on the front side of the HIT SSC, resulting in a large difference in EQE at the 300-700nm band [19].

Table 1 Performances of the bifacial HIT solar cell

Side	V_{OC} (V)	J_{SC} (mA/cm²)	*FF*	Efficiency (%)
Front	0.725	39.4	0.81	23.08
Rear	0.723	37.9	0.79	21.80

Additionally, the non-ideal diode factor m used for the estimation of the HIT SSC's V_{OC} under filtered illumination can be obtained by the results given in Figure 1(c). The slopes of fitting lines show *m*=1.23 for front side and *m*=1.24 for rear side of the HIT SSC, indicating excellent passivation and minimum non-radiative recombination. The value of m was set as 1.23 in the calculation.

3.2 *Ideal efficiency of 23%-efficient HIT-Si-cell-based tandem devices*

A 4-T tandem device with sub-cells coupling without optical losses can perform maximum efficiency in a certain configuration. For a reflective tandem

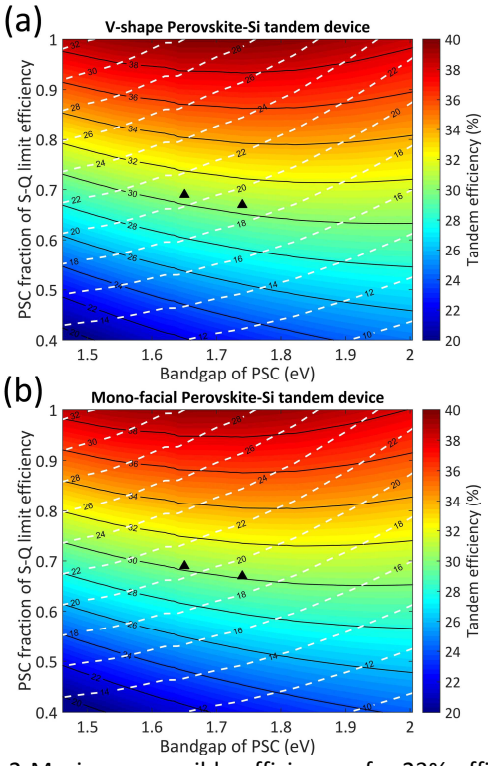

Figure 2 Maximum possible efficiency of a 23%-efficient-HIT-cell-based tandem as a function of the bandgap and the efficiency of PSCs. (a) V-shape tandem configuration. (b) Mono-facial tandem configuration.

configuration consisting of a practical bifacial HIT cell and ideal PSCs with S-Q limit efficiencies, an optical lossless couple requires f_{nb}=f_{pb}=0 and f_{nr}=f_{pr}=1 in Eq. (5). This means that the PSCs absorb all of the incident photons with energy higher than E_g, and reflect all of that with energy lower than E_g to the SSC.

In addition, a constant factor C (the fraction of PSC efficiency to S-Q limit efficiency) displayed in Eq. (2) can be used to multiply by the S-Q limit efficiency to represent the efficiency of a PSC that with reduced V_{OC}, FF, or $J_{SC}(\lambda)$ by the same fraction at each wavelength. Figure 2 shows the calculating efficiencies of 23%-efficient SSC-based tandem devices (V-shape and mono-facial reflective configuration) as a function of the bandgap of efficiency of PSC. The maximum efficiency of a V-shape device is 39.91% with an ideal PSC with bandgap of 1.74eV, and that of a mono-facial device is 39.57% with an ideal PSC with bandgap of 1.64eV. The increased V_{OC} of the silicon sub cell in V-shape configuration results in higher maximum ideal efficiency of the tandem device, and leads to a different require of optimized PSC's bandgap.

The triangle symbols marked in each plot represent the maximum possible efficiencies of the tandem devices using record PSCs with bandgap of 1.65eV and 1.74eV, which can all exceed 30% as listed in Table 2. Thanks to the V_{OC} improvement, the V-shape tandem devices with half amount of SSCs can perform even higher efficiency than the mono-facial tandem devices

Table 2 Maximum possible efficiencies of 4-T tandem devices pairing HIT SSC and record PSCs with different bandgap

PSC	E_g (eV)	Efficiency (%)	C	Tandem efficiency* (%)
1[20]	1.65	20.7	0.69	30.26 (30.59)
2[20]	1.74	19.1	0.67	30.15 (30.53)

*The tandem efficiencies in parentheses correspond to the V-shape configuration; those not in parentheses correspond to the mono-facial configuration.

3.3 *Predicting efficiency of a practical V-shape tandem device with the factor f*

In practical cases, the reflection characteristics of PSCs are generally non-ideal due to unwanted reflection at interfaces between layers or parasitic absorption in different layers. Optical simulation models of PSCs with typical n-i-p structure of TCO/SnO_2/Perovskite/Spiro-OMeTAD/Au are established as shown in Fig. 3(a) to investigate the effects of perovskite bandgap, thickness of TCO and spiro layers, as well as type of TCO (IWO or ITO) on the values of factor f. In this work, the thicknesses of SnO_2, perovskite, and Au layer for each simulation are set as 25nm, 550nm, and 150nm, respectively. The glass is assumed to be perfectly transparent with a constant refractive index of 1.53 as its thickness is much larger than that of the other layers. The incident angle is set as 45° in vacuum and adjusted to 27.52° in glass. The optical properties of ITO, SnO_2, perovskite ($Cs_yFA_{1-y}Pb(I_xBr_{1-x})_3$), Spiro-OMeTAD, and Au were taken from literature [21-25], and the optical

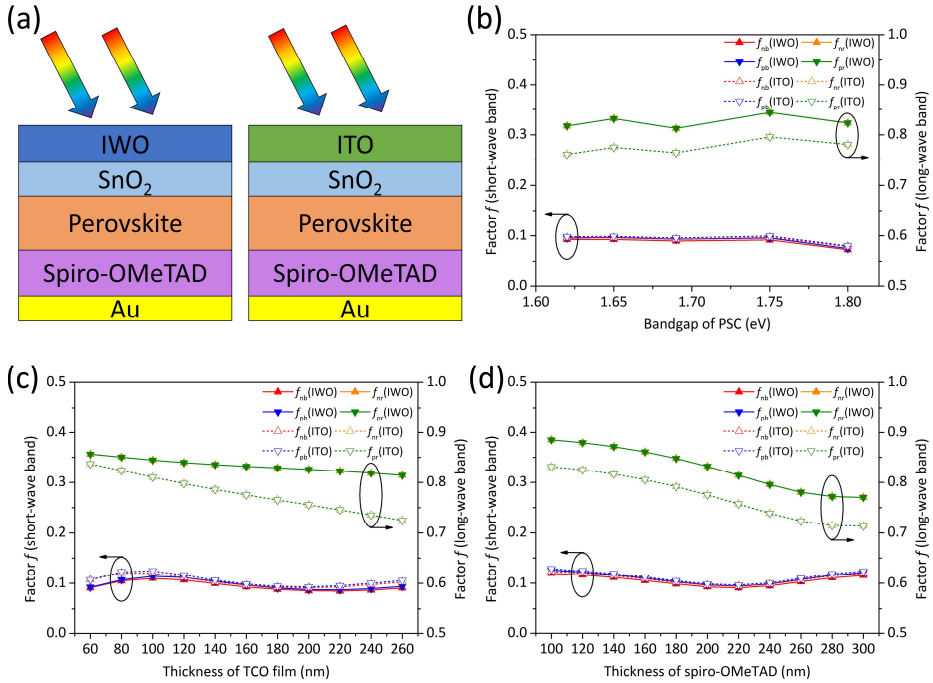

Figure 3(a) Diagram of PSCs structure for simulation. Calculated results of factor f with varying (b) bandgap of PSC, (c) thickness of TCO film (with 200nm spiro) and (d) thickness of spiro-OMeTAD (with 160nm TCO)

properties of IWO were obtained from spectroscopic ellipsometry measurements.

Figure 3(b) gives the calculation results of factor *f* as a function of varying bandgap of PSC. The thicknesses of TCO films and spiro-OMeTAD layer are set as 160nm and 200nm, respectively. It is apparent that both factor *f* for short-wave band (f_b) and factor *f* for long-wave band (f_r) are maintained within a small range of values without significant variation when the bandgap varies from 1.62 eV to 1.80 eV. This is similar to the results that calculated with the data obtained from literature [8]. In addition, the calculation results of factor *f* corresponding to varying thicknesses of TCO films (60 nm - 260 nm) and spiro-OMeTAD layer (100 nm - 300 nm) are plotted in Figure 3(c) and 3(d), respectively. It is surprised that the values of f_b are maintained at around 0.1 when the perovskite bandgap, thickness of TCO and spiro layers, or the type of TCO changes. However, as the thicknesses of TCO films and spiro-OMeTAD layer increase, the f_r decrease monotonically due to the enhanced parasitic absorption. Since IWO has a smaller parasitic absorption than ITO for infrared light, the f_r of the IWO based PSC is much higher and declines much more slowly with increasing TCO thickness. This means that changing the IWO thickness may have minor influences on the performance of HIT SSCs, which allows a more flexible adjustment of the sheet resistance and reflection spectrum based on the thickness of IWO.

According to the results of Figure 3, the values of factor *f* for the front and rear side of the tandem devices are almost equivalent. Based on the results discussed above, simplification can be made for Eq. (5) that $f_{nr}=f_{pr}=f_r$ and $f_{nb}=f_{pb}=f_b\approx0.1$. Therefore, with a given bandgap of PSC, we can make an efficiency prediction for a V-shape tandem device pairing non-ideal PSCs and a 23%-efficient HIT solar cell as a function of factor *C* and f_r, as plotted in Figure 4.

This plot helps to intuitively evaluate and compare PSCs from various dimensions of efficiency, layer thickness, and TCO type with the help of factor f_r, providing a guide for selecting and optimizing PSC's structure. For example, consider a 20.7%-efficient PSC with bandgap of 1.65eV, coupling with a 23%-efficient bifacial HIT SSC in a V-shape configuration. The pathway to reach the 30% tandem efficiency is to improve the f_r to over 0.82. For a PSC with the typical structure in Figure 3(a), when the thickness of the spiro layer is fixed at 200 nm, this requires the thickness of the IWO layer to be ≤220 nm (for ITO, ≤80 nm); when the thickness of the TCO is fixed to 160 nm, this requires the thickness of the spiro layer to be ≤200 nm (for IWO) or ≤120nm (for ITO). Furthermore, given the above results, it is evident that with a competitive conductivity, the IWO would be a more appropriate TCO for PSCs used in V-shape tandem.

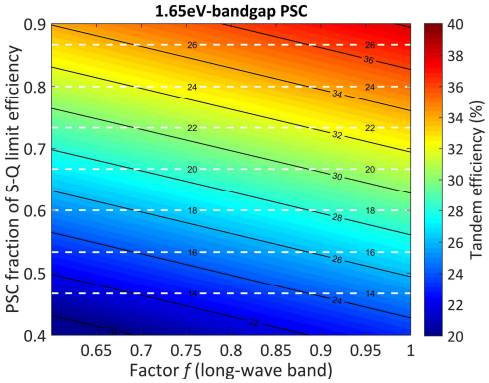

Figure 4 Predicted efficiency of a 23%-efficient-HIT-cell-based tandem as a function of the factor f_r and the efficiency of PSCs with bandgap of 1.65eV The dash contour white lines indicate the efficiency of the PSCs.

4. CONCLUSIONS

A comprehensive method was developed for performance estimation of a V-shape tandem device composed of a fabricated 23%-efficient bifacial HIT SSC. The ideal efficiency of tandem devices consisting of this Si cell and ideal PSCs are 39.91% with V-shape configuration and 39.57% with mono-facial tandem configuration, respectively. For the non-ideal condition, the effects of material parameters of a PSC with typical TCO/SnO2/perovskite/spiro-OMeTAD/Au structure on the tandem efficiency were evaluated uniformly with an introduced factor *f* that is positively related to the tandem efficiency. The f_r decreases monotonically as the thickness of TCO layer or spiro-OMeTAD layer increases due to parasitic absorption, and is very slightly affected by the PSC's bandgap.

In addition, IWO and ITO are compared as two kinds of TCO material of the PSCs during the calculation. It is noteworthy that, the f_r of IWO-based devices is much higher than that of ITO-based devices in all cases, and is affected much more slightly by the increasing thickness of TCO layer. Therefore, for PSCs paired with HIT SSCs in V-shaped tandem devices, IWO is a better choice for transparent electrode materials.

ACKNOWLEDGEMENT

This work was financially supported by the Basic Science Center Program for Ordered Energy Conversion of the National Natural Science Foundation of China (No. 51888103) and the National Natural Science Foundation of China (No. 51590901).

REFERENCE

[1] Kojima A, Teshima K, Shirai Y, Miyasaka T. Organometal halide perovskites as visible-light sensitizers for photovoltaic cells. J Am Chem Soc. 2009;131:6050-1.

[2] Kim HS, Lee CR, Im JH, Lee KB, Moehl T, Marchioro A, Moon SJ, Humphry-Baker R, Yum JH, Moser JE, Gratzel M, Park NG. Lead iodide perovskite sensitized all-solid-state submicron thin film mesoscopic solar cell with efficiency exceeding 9%. Sci Rep. 2012;2:591.

[3] Green MA, Dunlop ED, Hohl-Ebinger J, Yoshita M, Kopidakis N, Hao XJ. Solar cell efficiency tables (version 56). Prog Photovoltaics. 2020;28:629-38.

[4] Werner J, Niesen B, Ballif C. Perovskite/silicon tandem solar cells: Marriage of convenience or true love story?–An overview. Adv Mater Interfaces. 2018;5:1700731.

[5] Zhang ZH, Li ZC, Meng LY, Lien SY, Gao P. Perovskite-based tandem solar cells: Get the most out of the sun. Adv Funct Mater. 2020;n/a:2001904.

[6] Löper P, Niesen B, Moon S-J, De Nicolas SM, Holovsky J, Remes Z, Ledinsky M, Haug F-J, Yum J-H, De Wolf S. Organic–inorganic halide perovskites: Perspectives for silicon-based tandem solar cells. IEEE J Photovolt. 2014;4:1545-51.

[7] Duong T, Grant D, Rahman S, Blakers A, Weber KJ, Catchpole KR, White TP. Filterless spectral splitting perovskite–silicon tandem system with> 23% calculated efficiency. IEEE J Photovolt. 2016;6:1432-9.

[8] Li Y, Hu HW, Chen BB, Salim T, Zhang J, Ding JN, Yuan NY, Lam YM. Reflective perovskite solar cells for efficient tandem applications. J Mater Chem C. 2017;5:134-9.

[9] Duong T, Wu Y, Shen H, Peng J, Fu X, Jacobs D, Wang EC, Kho TC, Fong KC, Stocks M. Rubidium multication perovskite with optimized bandgap for perovskite-silicon tandem with over 26% efficiency. Adv Energy Mater. 2017;7:1700228.

[10] Wang Z, Zhu X, Zuo S, Chen M, Zhang C, Wang C, Ren X, Yang Z, Liu Z, Xu X, Chang Q, Yang S, Meng F, Liu Z, Yuan N, Ding J, Liu S, Yang D. 27%-Efficiency four-terminal perovskite/silicon tandem solar cells by sandwiched gold nanomesh. Adv Funct Mater. 2020;30:1908298.

[11] Da Y, Xuan Y, Li Q. Quantifying energy losses in planar perovskite solar cells. Sol Energ Mat Sol C. 2018;174:206-13.

[12] Reich NH, van Sark WGJHM, Alsema EA, Lof RW, Schropp REI, Sinke WC, Turkenburg WC. Crystalline silicon cell performance at low light intensities. Sol Energ Mat Sol C. 2009;93:1471-81.

[13] Zheng L, Wang J, Xuan Y, Yan M, Yu X, Peng Y, Cheng Y-B. A perovskite/silicon hybrid system with a solar-to-electric power conversion efficiency of 25.5%. J Mater Chem A. 2019;7:26479-89.

[14] Islam M, Wahid S, Alam MK. Physics-based modeling and performance analysis of dual junction perovskite/silicon tandem solar cells. Phys Status Solidi A. 2017;214:1600306.

[15] Yu ZSJ, Fisher KC, Wheelwright BM, Angel RP, Holman ZC. PVMirror: A new concept for tandem solar cells and hybrid solar converters. IEEE J Photovolt. 2015;5:1791-9.

[16] Yu ZS, Leilaeioun M, Holman Z. Selecting tandem partners for silicon solar cells. Nat Energy. 2016;1:16137.

[17] Zheng L, Xuan Y. Realization of omnidirectional ultra-broadband antireflection properties via subwavelength composite structures. Appl Phys B-Lasers O. 2017;123:263.

[18] Zheng L, Xuan Y. Suppressing the negative effect of UV light on perovskite solar cells via photon management. Sol Energy. 2018;173:1216-24.

[19] Paduthol A, Juhl MK, Nogay G, Loper P, Trupke T. Measuring carrier injection from amorphous silicon into crystalline silicon using photoluminescence. Prog Photovoltaics. 2018;26:968-73.

[20] Tan H, Che F, Wei M, Zhao Y, Saidaminov MI, Todorović P, Broberg D, Walters G, Tan F, Zhuang T, Sun B, Liang Z, Yuan H, Fron E, Kim J, Yang Z, Voznyy O, Asta M, Sargent EH. Dipolar cations confer defect tolerance in wide-bandgap metal halide perovskites. Nat Commun. 2018;9:3100.

[21] Holman ZC, Filipic M, Descoeudres A, De Wolf S, Smole F, Topic M, Ballif C. Infrared light management in high-efficiency silicon heterojunction and rear-passivated solar cells. J Appl Phys. 2013;113:013107.

[22] Ball JM, Stranks SD, Horantner MT, Huttner S, Zhang W, Crossland EJW, Ramirez I, Riede M, Johnston MB, Friend RH. Optical properties and limiting photocurrent of thin-film perovskite solar cells. Energy Environ Sci. 2015;8:602-9.

[23] Werner J, Nogay G, Sahli F, Yang TC-J, Bräuninger M, Christmann G, Walter A, Kamino BA, Fiala P, Löper P, Nicolay S, Jeangros Q, Niesen B, Ballif C. Complex refractive indices of cesium–formamidinium-based mixed-halide perovskites with optical band gaps from 1.5 to 1.8 eV. ACS Energy Lett. 2018;3:742-7.

[24] Filipič M, Löper P, Niesen B, De Wolf S, Krč J, Ballif C, Topič M. CH3NH3PbI3 perovskite / silicon tandem solar cells: characterization based optical simulations. Opt Express. 2015;23:A263-A78.

[25] Rakic AD, Djurisic AB, Elazar J, Majewski ML. Optical properties of metallic films for vertical-cavity optoelectronic devices. Appl Optics. 1998;37:5271-83.